Preparation of Biomimetic-Bone Materials and Their Application to the Removal of Heavy Metals

Bo Sun, Hui-Yun Tian, Chun-Xue Zhang and Gang An
School of Chemistry and Chemical Engineering, Tianjin University of Technology, Tianjin, 300384, P.R. China

DOI 10.1002/aic.13802
Published online April 12, 2012 in Wiley Online Library (wileyonlinelibrary.com).

Since heavy metals react with some components in bone, it can be surmized that these components would strongly fix heavy metals. Hydroxyapatite and a series of substituted-apatites that are likely to exist in bone were prepared under near-physiological conditions with the aim of developing materials that are capable of effectively removing low concentrations of heavy-metal ions at near-neutral conditions. The obtained apatites were characterized by inductively coupled plasma optical emission spectroscopy, Fourier transform infrared spectroscopy, X-ray diffractometry, thermogravimetric and differential thermal analysis, and field-emission scanning electron microscopy. They were also tested for their ability to remove Pb, Cd, Hg, Cr, and As. The carbonate-substituted apatite exhibited very strong fixation of Pb^{2+}, Cd^{2+}, and Cr^{3+}, and moderately strong fixation of Hg^{2+}. Based on a heavy-metal-fixing mechanism, a bone-like composite, with chitosan as the saccharide portion and a polyaspartyl polymer as the protein portion, was synthesized via co-precipitation. The biomimetic composite was excellent at removing Pb^{2+}, Cd^{2+}, Hg^{2+}, and Cr^{3+}, with removal percentages as high as 99.8% and residual concentrations as low as 0.01 mg/L. However, the composite had little fixation of $Cr_2O_7^{2-}$, CrO_4^{2-}, or H_3AsO_3. When Cr(VI) was reduced to Cr(III), the percent removed increased greatly. © 2012 American Institute of Chemical Engineers *AIChE J,* 59: 229–240, 2013
Keywords: bone-resembling biomimetic material, substituted-apatites, heavy metals

Introduction

Heavy-metals (such as Pb, Cd, Hg, As, and Cr) are very harmful to living organisms.[1–6] Their actions are believed to be due to their interactions with the chemical components in the organisms, which seriously affect the organism's normal physiological functions.[7–15] This suggests that the components in cell walls, cell membranes, proteins, enzymes, and bones are sensitive to trace concentrations of heavy metals, that is, these structures strongly fix heavy metals. Based on this "heavy-metal poisoning mechanism," biomimetic-materials capable of removing trace heavy-metals have been developed.

In our previous work,[16,17] biomimetic materials with a protein-like structure and with a peptide-polysaccharide-like structure that is similar to plant cell walls/membranes were developed, and the structure-activity relationship between them and heavy metals was investigated. These materials were excellent binding agents when the concentration of heavy-metal ions was high. However, when the concentration of heavy-metal ions was low (<1 mg/L), they were less effective for the removal of heavy metals. This is because the adsorption equilibrium constant is not very high which limits the amount of heavy metal ions which can be removed.

Inspired by the phenomenon that heavy metals react with some components in bone,[9,12] we shifted our attention to these components. In addition to proteins and other organic substances, there are a large number of inorganic salts (bone salts) in human bone. Using the elements found in bone (e.g., calcium, magnesium, strontium, phosphorus, fluorine, and carbon) and the other components of human bone,[18–22] some bone-salt-like inorganic compounds which are likely to exist in bone were prepared under near-physiological conditions. Furthermore, a bone-like composite, with chitosan as the saccharide portion and polyasparte as the protein portion, was also prepared. The behavior of the obtained materials for the fixation of heavy metals was examined with an aim of determining the mechanism of fixing heavy metals to bone. In addition, useful information for designing materials that can effectively remove heavy metals at low concentrations under near-neutral conditions was obtained.

Experimental

The reagents and materials

Polysuccinimide (PSI) and polyaspartate hydrogel were prepared according to the method reported in the literature.[16] Chitosan powder, with a deacetylation degree of 90−95%, was supplied by Zhejiang Yongyue Ocean Biology (Zhejiang Province, China).

D380 (weakly basic anion exchanger-primary amine functionality, macroporous type), D382 (weakly basic anion exchanger-secondary amine functionality, macroporous type), and D301R (weakly basic anion exchanger-tertiary amine functionality, macroporous type) were purchased from Tianjin Nankai Hecheng S & T (Nankai Group, China).

Correspondence concerning this article should be addressed to B. Sun at sunbo_tjlg@hotmail.com.

Table 1. Instrumental Parameters and Operating Conditions for ICP-OES

Radio frequency (R.F.) power	1.2 kW
Plasma gas flow rate	15 L/min
Flow rate of Argon auxiliary	1.5 L/min
Nebulizer gas flow rate	0.9 L/min
Precision (general)	1−3%
Detection limit	0.01 mg/L
Pb analytical line (λ)	220.3 nm
Cd analytical line (λ)	226.5 nm
Hg analytical line (λ)	184.9 nm
Cr analytical line (λ)	267.7 nm
As analytical line (λ)	193.6 nm
Ca analytical line (λ)	396.8 nm
Mg analytical line (λ)	279.6 nm
Sr analytical line (λ)	407.8 nm
P analytical line (λ)	213.6 nm

All other reagents were obtained from Tianjin Chemical Reagent (Tianjin, China), were analytical grade and were used as received.

Measurements

The total concentrations of heavy-metal ions in the aqueous solutions were determined with a Vista MPX inductively coupled plasma optical emission spectroscopy (ICP-OES) Spectrometer (Varian, Palo Alto, CA). The instrumental operating conditions are shown in Table 1.

The fluoride content of the samples was measured using a solid-state fluoride selective electrode coupled to a Model pHS-25 pH Meter (Shanghai Rex Instruments Factory, Shanghai, China) with a 0.01-mV resolution. The potentials between the fluoride-ion-selective electrode and the saturated calomel electrode were recorded, and the amount of F^- remaining in the aqueous solution after precipitation was determined using a calibration curve of potential vs. log of the F^- concentration. The fluoride content of the samples was determined by calculating the difference between the amount of F^- added before reaction and that left in the solution after the reaction.

The amount of carbon in the samples was determined using a vario-EL element analyzer (Elementar Analysensysteme GmbH). The precision of the results was estimated to be 0.3%.

Fourier transform infrared (FT-IR) spectra were recorded with a Nicolet Magna-560 FTIR spectrometer (Madison, WI) in KBr pellets over a range of 4000–400 cm^{-1} with a 4-cm^{-1} resolution.

The thermogravimetric (TG) and differential thermal analysis (DTA) were performed with a Rigaku standard TG-DTA analyzer at a heating rate of 10°C /min up to 700–1000°C in nitrogen gas (initial pressure of 0.1 bar), and using α-Al_2O_3 as the reference.

Powder X-ray diffraction (XRD) patterns were recorded on a Rigaku D/MAX-2000PC X-ray diffractometer, with Cu Kα radiation ($\lambda = 0.154$ nm) at 100 mA and 40 kV. A scan rate of 10°C/min and a step size of 0.02° were used over a 2θ range of 10–90°.

The surface morphology of the samples was observed with a JEOL JSM-6700F field-emission scanning electron microscopy (FE-SEM) (JEOL Ltd., Tokyo, Japan). The compositions of the samples were evaluated using energy dispersive spectrometry (EDS) using an Oxford-EDS7421 apparatus. The samples were mounted on a copper conductive tape and coated with Au to minimize sample charging.

X-ray photoelectron spectroscopy (XPS) was performed with a PerkinElmer PHI-1600 electron-spectroscopic-chemical analyzer (Wellesley, MA) equipped with a hemispherical electron energy analyzer and a Mg Kα monochromator source [light Quantum energy ($h\nu$) = 1253.6 eV]. The pressure in the analysis chamber during data acquisition was $\sim 10^{-7}$ Pa. The analysis area was 0.8 mm^2. The survey spectra were performed with a pass-energy of 187.85 eV. The contaminant C1s peak at 284.6 eV was used to calibrate the energy shift. The accuracy of the binding energy is estimated to be $\pm$0.2 eV. All spectral data was treated with PHI Multipak software (version 6.0, Wellesley, MA).

Preparation of hydroxyapatite and substituted apatites

The preparation of hydroxyapatite and some substituted-apatites has been reported in the literature.[23–28] To obtain bone salts that are likely to exist in human bones, a method of preparing the salts under near-physiological conditions, that is, at 36−40°C and pH 7.2−7.5 was adopted.

Preparation of hydroxyapatite (HAP or CaHAP)

Hydroxyapatite was prepared by precipitation from a dilute solution according to a method reported in the literature.[24] The general procedure is as follows:

A $Ca(NO_3)_2$ solution was prepared by dissolving 0.316 g of $Ca(NO_3)_2{\cdot}4H_2O$ (ca. 1.34 mmol Ca) in 400 mL of deionized water, and a Na_2HPO_4 solution by dissolving 0.287 g of $Na_2HPO_4{\cdot}12H_2O$ (ca. 0.80 mmol P) in 400 mL of deionized water. The pH of each solution was adjusted to 7.2−7.5 by the addition of NaOH or HNO_3, as needed.

Under vigorous stirring, the two above solutions were mixed thoroughly in a 1000-mL four-necked round-bottomed flask equipped with a thermometer, condenser, and mechanical stirrer. The mixture was heated to 36−40°C with agitation and the temperature was maintained until the solution became turbid and its pH became more acidic. Then, 0.1 mol/L NaOH solution was added dropwise to control the pH value of the mixture at 7.2−7.5 until no further change in pH was observed with time. Then, the mixture was stirred for another 3 h to ensure a complete reaction. After being cooled to room temperature, the precipitate was centrifuged, washed several times with deionized water, and dried at 130°C to a constant weight. About 0.134 g of solid was obtained [the theoretical yield is 0.134 g, assuming the product is pure $Ca_{10}(OH)_2(PO_4)_6$].

Preparation of strontium-substituted apatite (Sr-AP)

Sr-AP was prepared by a method similar to that for the preparation of HAP, except that 0.284 g (1.34 mmol) of $Sr(NO_3)_2$ was substituted for the $Ca(NO_3)_2{\cdot}4H_2O$. About 0.198 g of solid was obtained [theoretical yield is 0.198 g, assuming the product is pure $Sr_{10}(OH)_2(PO_4)_6$].

Preparation of Magnesium-substituted apatite (Mg-AP)

Mg-AP was prepared by a method similar to that for HAP, except that 0.163 g of anhydrous $MgSO_4$ was substituted for $Ca(NO_3)_2{\cdot}4H_2O$. About 0.025 g of solid was obtained [theoretical yield is 0.113 g, assuming the product is pure $Mg_{10}(OH)_2(PO_4)_6$].

Preparation of fluoride-substituted apatite (F-AP)

According to the stoichiometric Ca:P:F (5:3:1) mole ratio in the substituted apatite that we want to prepare, 1.033 g of $Ca(NO_3)_2{\cdot}4H_2O$ (ca. 4.37 mmol Ca) was dissolved in 100

Table 2. Elemental Analyses of the Prepared Phosphates

Phosphates Obtained	M/P* (mol/mol)	F/C Content (wt %)	Yield of Product/Theoretical Amount† (g/g)
Calcium-containing phosphate	1.72	–	0.134/0.134
Strontium-containing phosphate	1.62	–	0.198/0.198
Magnesium-containing phosphate	1.60	–	~ 0.025/0.113
Calcium-fluoride-containing phosphate	1.60	3.3 (F content)	0.442/0.441
Calcium-carbonate-containing phosphate	1.61	1.5 (C content)	0.468/0.477

*M = Ca, Sr or Mg, initial C (M^{2+}) = 3.34 mmol/L, initial C (P) = 2.00 mmol/L, initial C (F^-) = 0.67 mmol/L, initial C(HCO_3^-) = 0.67 mmol/L, 36−40 °C, pH = 7.2−7.5
†Theoretical amount was calculated based on appropriate substituted-apatite

mL of deionized water, 0.938 g of $Na_2HPO_4{\cdot}12H_2O$ (ca. 2.62 mmol P) in 300 mL of deionized water, and 0.037 g of NaF (ca. 0.88 mmol F) in 300 mL of deionized water. The pH of each solution was adjusted to 7.2−7.5 by the addition of NaOH or HNO_3, as needed.

Under vigorous stirring, the Na_2HPO_4 and NaF solutions were mixed thoroughly in a 1000-mL four-necked round-bottomed flask equipped with a thermometer, condenser, and mechanical stirrer. The mixture was heated to 36−40°C with agitation, and then, the $Ca(NO_3)_2$ solution was added dropwise to the flask at a rate of about 20 mL/h. At the same time, 0.1 mol/L NaOH was added dropwise to control the pH of the mixture at 7.2−7.5 until the $Ca(NO_3)_2$ solution had been completely added to the flask, and there was no change in pH observed with time. The contents of the flask were then stirred for 3 h to ensure a complete reaction. After being cooled to room temperature, the precipitate was centrifuged, washed several times with deionized water, and dried at 130°C to a constant weight. About 0.442 g of a solid was obtained [theoretical yield is 0.441 g, assuming the product is pure $Ca_{10}F_2(PO_4)_6$].

Preparation of carbonate-substituted apatite (HCO_3-AP)

Carbonate-substituted apatite powder was prepared by a method similar to that for F-AP, except that 0.074 g of $NaHCO_3$ was substituted for NaF. About 0.463 g of solid was obtained [theoretical yield is 0.477 g, assuming the product is pure $Ca_{10}(HCO_3)_2(PO_4)_6$].

Preparation of chitosan-polyaspartyl polymer bone–like composite

Chitosan, PSI, H_3PO_4, and $CaCl_2$ were used as the starting materials. The chitosan-polyaspartate-containing bone-like composite was synthesized by a co-precipitation method. The general procedure is as follows.

A solution of chitosan was prepared by dissolving 0.1 g of chitosan powder in a combined solvent of 2.0 mL of 2 wt % aqueous acetic acid and 4 mL of 6.7 wt % H_3PO_4 (ca. 2.74 mmol P) aqueous solution. A polyaspartyl polymer, with amino groups on the side chain, was prepared according to the method in the literature.[16] Polyaspartyl polymer (0.1 g) was dissolved in 5 mL of deionized water and acidified to a pH of approximately 4−5 with dilute hydrochloric acid. The two solutions were mixed thoroughly under vigorous stirring and maintained at room temperature for 15 min, and then 0.2 mL of 50 wt % glutaraldehyde was added.

A $CaCl_2$ solution was prepared by dissolving 0.566 g of anhydrous $CaCl_2$ (5.10 mmol Ca) in 10 mL of water, and then was added to the chitosan-polyaspartyl polymer solution.

Next 0.043 g of $NaHCO_3$ and 1 mL of 6.7 wt % H_3PO_4 (ca. 0.68 mmol P) were added to a vessel with 25 mL of water, and the solution was adjusted to a pH of approximately 7.2−7.5 with NaOH. Then, under vigorous stirring, the above $CaCl_2$–chitosan–polyaspartyl polymer solution was added dropwise to the vessel. The temperature of the vessel was maintained at 36−40°C and the pH of the mixture was kept at 7.2−7.5 by adding 5 wt % aqueous NaOH. After all the solutions were added and complete precipitation was achieved (about 6 h), the resulting solid was allowed to stand at room temperature overnight. Afterwards, the precipitate was isolated and washed several times with deionized water until the pH of the washing medium was neutral. Then, the solid was dried at 40°C in vacuo to a constant weight. About 0.71 g of an orange-pink material was obtained.

Results and Discussion

Characterization of substituted apatites

Hydroxyapatite, $Ca_{10}(OH)_2(PO_4)_6$, is believed to be the principal component of bone[18] and has attracted a great deal of attention as a biomaterial. In addition to Ca^{2+}, HPO_4^{2-},

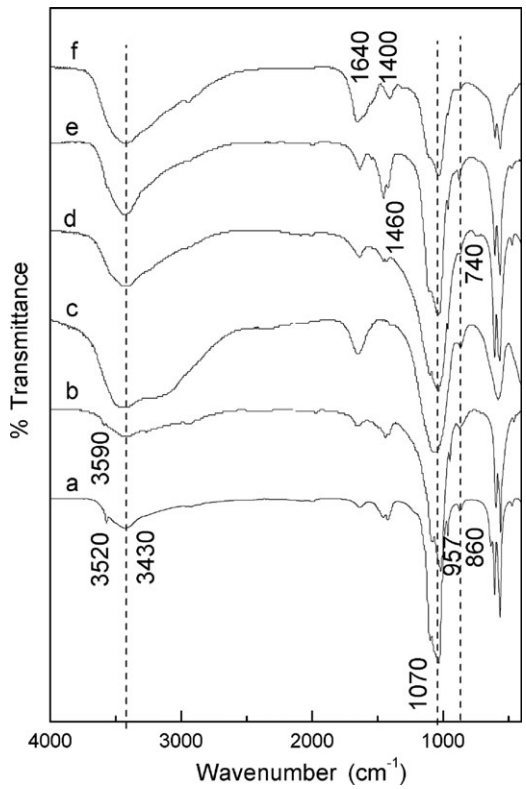

Figure 1. FT-IR spectra of the prepared phosphates containing (a) calcium (b) strontium (c) magnesium (d) calcium-fluoride (e) calcium-carbonate and (f) the composite.

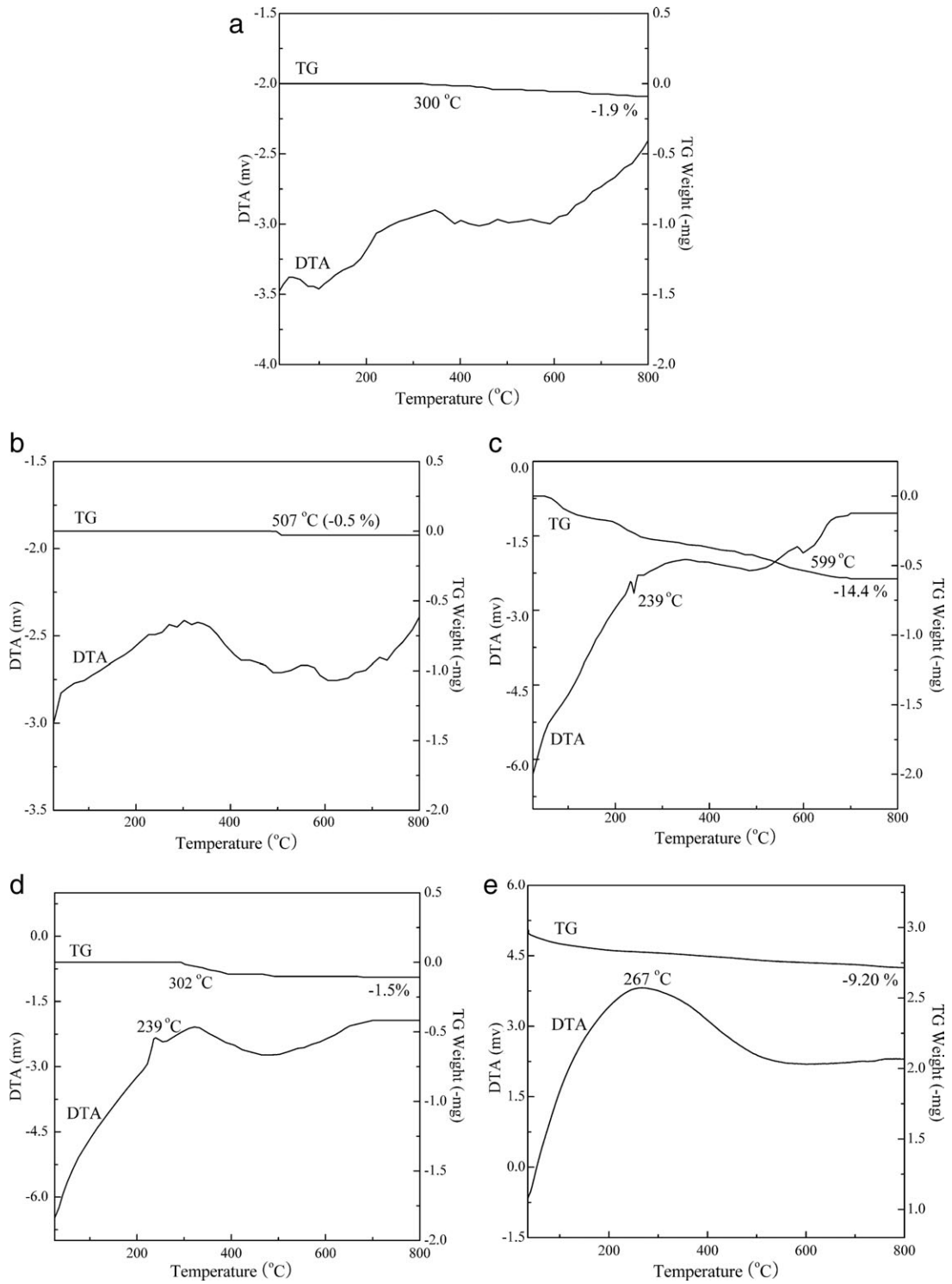

Figure 2. TG-DTA curves of the prepared phosphates containing (a) calcium (b) strontium (c) magnesium (d) calcium-fluoride and (e) calcium-carbonate.

and PO_4^{3-}, there are other cations and anions in the bones and body fluids of living organisms, such as Mg^{2+} and Sr^{2+}, as well as Cl^-, F^-, HCO_3^-, and SO_4^{2-}. In the crystal lattice of $Ca_{10}(OH)_2(PO_4)_6$, the Ca^{2+} ions can be exchanged with cations, and the OH^- and PO_4^{3-} ions can be substituted with other anions.[19–22] To determine which component in bone possesses the strongest ability to fix heavy metals, the heavy-metal-fixing ability of hydroxyapatite and the prepared substituted apatites was investigated. Table 2 lists the elemental analyses of the prepared phosphates. Figures 1–4 show their FT-IR spectra, TG-DTA curves, XRD patterns, and surface morphologies, respectively.

Characterization of the calcium-containing phosphate

Table 2 shows that the calcium-containing phosphate has a Ca/P molar ratio of 1.72, which is close to the stoichiometric atom ratio in hydroxyapatite. The FT-IR spectrum of the calcium-containing phosphate (Figure 1a) has an absorption

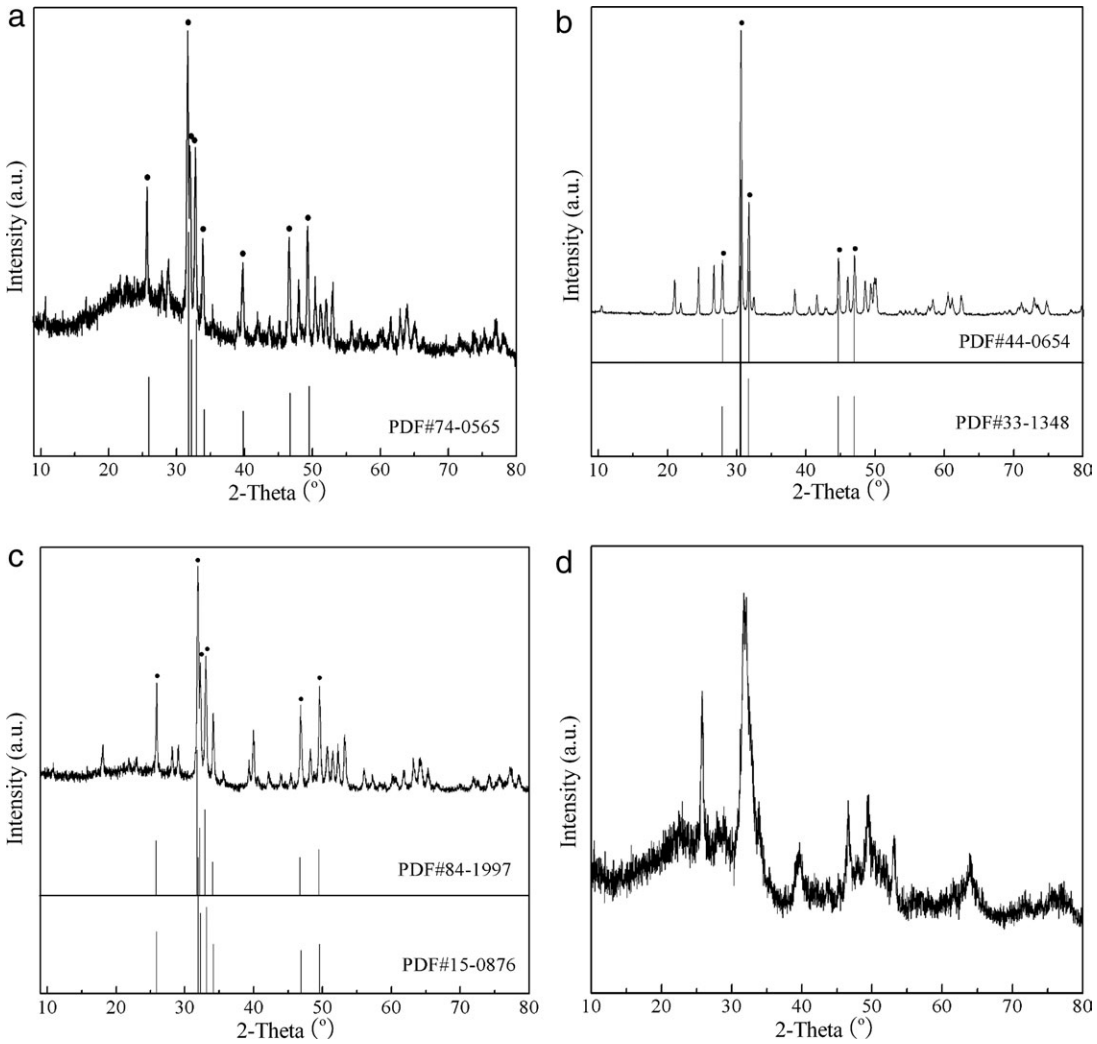

Figure 3. XRD patterns of the prepared phosphates containing (a) calcium (b) strontium (c) calcium-fluoride and (d) calcium-carbonate.

band around 3560 cm^{-1} which can be attributed to OH^- stretching vibrations and the absorption bands at 1070, 957, and 860 cm^{-1} are due to PO_4^{3-} stretching vibrations.[29] Figure 2a shows a 1.9% weight-loss in the sample which coincides with a 1.8% total water loss due to the thermal decomposition of $Ca_{10}(OH)_2(PO4)_6$. This serves as further evidence that the obtained calcium-containing phosphate is hydroxyapatite. The XRD pattern of the calcium phosphate sample (Figure 3a) has peaks at $2\theta = 25.78°$, $31.78°$, $32.10°$, $32.90°$, and $33.98°$ which are all characteristic peaks of hydroxyapatite (PDF#74-0565). However, the crystallinity of the sample is poor and there are indications of amorphous grains. From the elemental analysis, FT-IR, XRD, and TG-DTA results, it can be concluded that the obtained calcium-containing phosphate is hydroxyapatite. The obtained hydroxyapatite has a short rod-like appearance, as shown in Figure 4a.

Characterization of the strontium-containing phosphate

The strontium-containing phosphate has a Sr/P molar ratio of 1.62 (Table 2) which is close to the stoichiometric atom ratio in apatite. The FT-IR spectrum of the strontium-containing phosphate (Figure 1b) has a weak absorption at 3590 cm^{-1} which can be attributed to OH^- stretching vibrations, and the absorption bands at 1020, 943, and 868 cm^{-1} are due to PO_4^{3-} stretching vibrations.[29] The TG-DTA curves of the strontium-containing phosphate (Figure 2b) shows a rapid weight loss at about 507°C which is due to the loss of water in its structure. The 0.5% weight loss is obviously lower than the 1.2% total loss of water that would occur for $Sr_{10}(OH)_2(PO_4)_6$. The XRD pattern of the strontium-containing phosphate sample (Figure 3b) has peaks at $2\theta = 27.82°$, $30.50°$, $31.64°$, $44.60°$, and $46.92°$ which are characteristic peaks for $Sr_{10}(OH)_2(PO_4)_6$ (PDF#33-1348) and $Sr_{10}O(PO_4)_6$ (PDF#44-0654). However, the peaks are a better fit with the latter. From these results, it can be concluded that the obtained strontium-containing phosphate is a mixture of $Sr_{10}(OH)_2(PO_4)_6$ and $Sr_{10}O(PO_4)_6$ (Sr-AP). The sample is more crystalline than the hydroxyapatite obtained at the same temperature. Figure 4b shows that the strontium-substituted phosphate has a slender rod-like appearance.

Characterization of the magnesium-containing phosphate

The magnesium-containing phosphate has an Mg/P ratio of 1.60 (Table 2) which is close to stoichiometric atom ratio in apatite. For comparison, a magnesium-containing phosphate was also prepared at ~100°C. This was done to determine if the magnesium-containing apatite can exist at a high

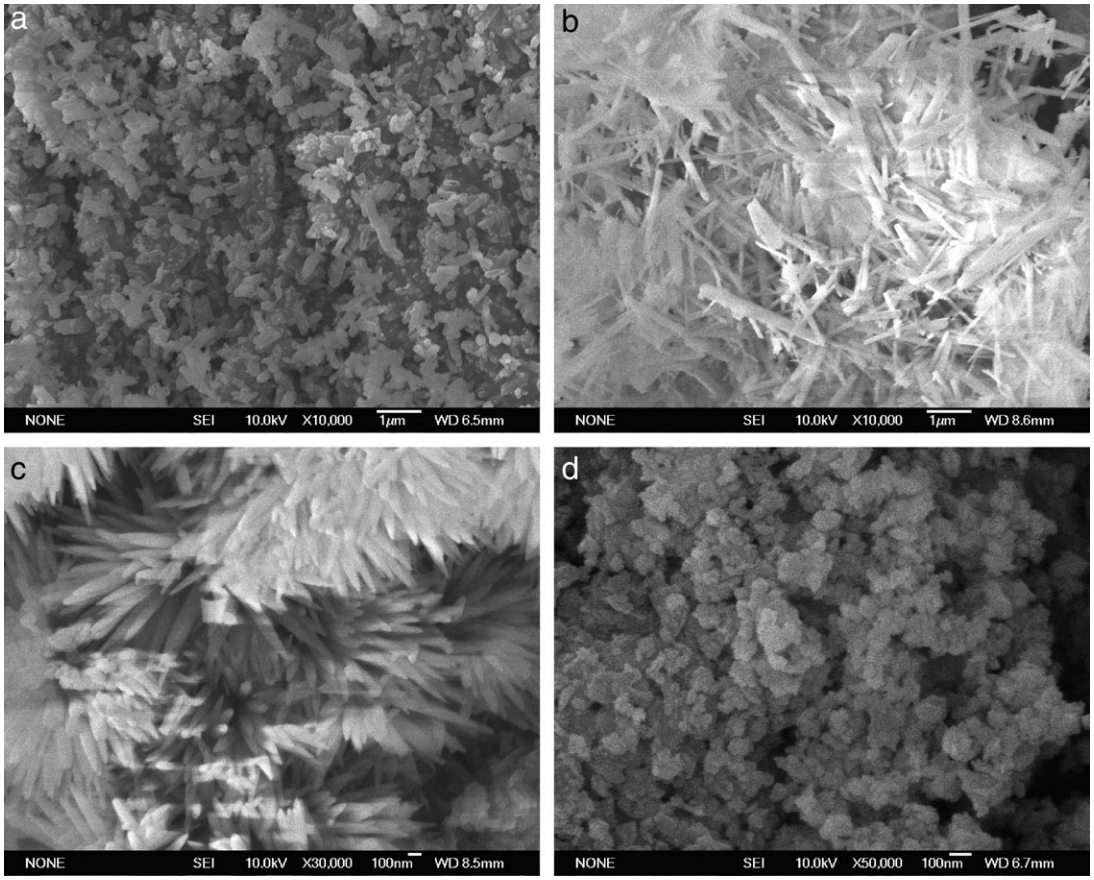

Figure 4. SEM photomicrographs of the prepared phosphates containing (a) calcium (b) strontium (c) calcium-fluoride and (d) calcium-carbonate.

temperature or if it could be prepared in a purer form (similar samples were also prepared for the calcium-fluoride-containing and calcium-carbonate-containing samples). The magnesium-containing phosphate obtained at ~100°C had a Mg/P ratio of 1.50. Only a very small amount of precipitate was obtained in the preparation of the magnesium-containing phosphate at 36–40°C, suggesting that even if a magnesium-substituted apatite exists, its solubility in water is too high for it to be a good adsorbent for the removal of heavy metals from aqueous solutions. From this result, we can also deduce that trace magnesium is unlikely to precipitate on bones.

The FT-IR spectrum of the magnesium-containing phosphate (Figure 1c) is different from the above phosphates. Whether obtained under near-physiological conditions or at a high temperature, there is no characteristic OH^- stretching band at ~3560 cm^{-1}. However, there is a strong broad band at 3440 cm^{-1} which is associated with the O—H stretching vibrations of water. The TG-DTA curves of the magnesium-containing phosphate obtained at 36–40°C (Figure 2c) show a gradual weight loss beginning at about 80°C. The 14.4% weight-loss in the temperature region of 0–700°C is far greater than the 2.13% total loss of water that would occur for $Mg_{10}(OH)_2(PO_4)_6$. This suggests that the obtained magnesium-containing phosphate is unlikely to be $Mg_{10}(OH)_2(PO_4)_6$. The XRD pattern for the magnesium-containing phosphate obtained at 36–40°C exhibits an amorphous pattern (not shown), and the magnesium-containing phosphate prepared at ~100°C is identical to $Mg_3(PO_4)_2{\cdot}8H_2O$ (2θ =11.06°, 12.70°, 29.70°, and 37.26°; PDF#84-1147). From the elemental analyses, FT-IR, XRD and TG-DTA results, it can be concluded that it is difficult to obtain a magnesium-substituted apatite from a dilute aqueous solution, and the magnesium-containing phosphate obtained at ~100°C is $Mg_3(PO_4)_2{\cdot}8H_2O$.

Table 3. The Unit Cell Dimensions and Volumes of Hydroxyapatite and Substituted Apatites

Apatites	a (nm)	b (nm)	c (nm)	V (nm^3)
Hydroxyapatite	0.9416	0.9416	0.6866	0.5271
Strontium-substituted apatite	0.9752	0.9752	0.7266	0.5984
Fluoride-substituted apatite	0.9383	0.9383	0.6880	0.5246
Carbonate-substituted apatite	0.9402	0.9402	0.6869	0.5260

Characterization of the calcium-fluoride-containing phosphate

The calcium-fluoride-containing phosphate has a Ca/P molar ratio of 1.60 (Table 2) which is close to the stoichiometric atom ratio in apatite. The fluoride elemental analysis indicates that the F-content in the product is about 88% of the theoretical amount [assuming the product is $Ca_{10}F_2(PO_4)_6$]. In contrast, the F-content in the product prepared at ~100°C was about 78% of theoretical amount suggesting that a relatively high temperature is unfavorable for the substitution of OH^- with F^-.

The FT-IR spectrum of the calcium-fluoride-containing phosphate (Figure 1d) does not have an obvious peak for OH^- stretching around 3560 cm^{-1}. In contrast, the spectrum of the calcium-fluoride-containing phosphate prepared at

Table 4. The Removal of Heavy Metals by Substituted Apatites

Adsorbents*	Final Concentration of M in Solution† (mg/L)						M-Removed (%)					
	Pb^{2+}	Cd^{2+}	Hg^{2+}	Cr^{3+}	Cr^{6+}	As^{3+}	Pb^{2+}	Cd^{2+}	Hg^{2+}	Cr^{3+}	Cr^{6+}	As^{3+}
HAP‡	48.04	34.15	15.98	16.05	24.90	35.90	51.7	36.7	83.4	35.7	0.0	0.0
Sr-HAP‡	0.10	35.94	19.35	14.53	24.90	35.90	99.9	33.4	79.9	41.8	0.0	0.0
F-AP‡	63.45	40.04	16.95	22.29	24.90	35.90	36.2	25.8	82.4	10.7	0.0	0.0
HCO_3^--AP‡	≤0.01	0.32	13.19	0.75	24.90	35.90	≥99.9	99.4	86.3	97.0	0.0	0.0
$Ca_3(PO_4)_2$§	≤0.01	1.24	17.33	2.80	24.90	35.90	≥99.9	97.7	82.0	88.8	0.0	0.0
$CaCO_3$§	13.53	21.6	77.80	0.37	24.90	35.90	86.4	60.0	19.2	98.5	0.0	0.0
Polyaspartate hydrogel	25.16	12.68	23.89	4.71	24.90	35.90	74.7	76.5	75.1	81.1	0.0	0.0

*Amount of adsorbents = 0.1 g, total volume of solution = 50 mL, pH = 6–7, exchange time = 2 h, temperature = 18°C, M = Pb, Hg, Cd, Cr, or As
†Initial concentration: $c\ (Pb^{2+}) = c\ (Cd^{2+}) = c\ (Hg^{2+}) = c\ (Cr^{3+}) = c\ (Cr^{6+}) = c\ (As^{3+}) = 0.48$ mmol/L, Cr^{6+} and As^{3+} were mainly in the form of $Cr_2O_7^{2-}$ or CrO_4^{2-} and $H_3AsO_3/HAsO_2$, respectively.
‡HAP and the substituted-apatites were unground, grain-sizes can be estimated from SEMs in Figure 4.
§The grain-size was about 40–50 μm.

~100°C has a small absorption band at 3538 cm^{-1} (not shown). The absorption band at 740 cm^{-1} is attributed to OH···F stretching vibrations,[30] and the absorption bands at 1030, 960, and 868 cm^{-1} are due to PO_4^{3-} stretching.

The TG-DTA curves of the calcium-fluoride-phosphate obtained at 36–40°C (Figure 2d) displays a rapid weight loss at 302°C. This can be attributed to the loss of water that is present in the crystal lattice due to strong H-bonding between F and H_2O. The XRD pattern of the calcium-fluoride-phosphate obtained at 36–40°C (Figure 3c) has peaks at $2\theta = 25.84°$, 31.82°, 32.20°, 33.00°, and 49.52° which are not in accordance with the characteristic peaks of $Ca_5(PO_4)_3F$ (PDF#15-0876), but which are characteristic for $Ca_5(PO_4)_3F_{0.94}Cl_{0.1}$ (PDF#84-1997). This is because the $Ca_5(PO_4)_3F$ in the database was obtained at 1000°C,[30] whereas our sample was prepared at 36–40°C, and thus, has a different crystal lattice structure.

From these results, it can be concluded that the calcium-fluoride-phosphate obtained at 36–40°C is $Ca_5(PO_4)_3F_{0.88}(OH)_{0.12}$. The fluoride-substituted apatite is more crystalline than hydroxyapatite, and exhibits a pine needle-like appearance, as shown in Figure 4c.

Characterization of the calcium-carbonate-containing phosphate

Table 2 shows that the calcium-carbonate-containing phosphate has a Ca/P molar ratio of 1.61 which is close to stoichiometric atom ratio in apatite. The FT-IR spectrum of the calcium-carbonate-containing phosphate (Figure 1e) does not have an obvious characteristic OH^- stretching band around 3560 cm^{-1}, but does have a strong band at 1460 cm^{-1} which can be assigned to HCO_3^- anion stretching vibrations.[31] The absorption bands at 1030, 958, and 870 cm^{-1} are due to phosphate anions. In contrast, the spectrum of the calcium-carbonate-containing phosphate prepared at ~100°C has an absorption band at 3564 cm^{-1} (not shown).

The TG-DTA curves (Figure 2e) of the calcium-carbonate-containing phosphate obtained at 36–40°C show a notable weight-loss at 267°C, which is attributed to the loss of the CO_2 and H_2O that are formed during the thermal decomposition of carbonate. The 9.2% total weight-loss of the sample in the range of 0–1000°C is in good agreement with the expected 9.7% total loss that would occur for $Ca_{10}(HCO_3)_2(PO_4)_6$.

The XRD pattern of the calcium-carbonate-phosphate obtained at 36–40°C (Figure 3d) exhibits a similar pattern to that of hydroxyapatite, with characteristic peaks at $2\theta = 25.84°$, 31.78°, and 32.08°. However, it has poor crystallinity and smaller crystal grains than hydroxyapatite which is known from the smaller peak-widths at half height. No characteristic peaks for $CaCO_3$ were observed.

From these results, it can be concluded that the obtained calcium-carbonate-phosphate is likely to be a HCO_3^--substituted apatite. In addition a relatively high temperature is unfavorable for the substitution of OH^- with HCO_3^- but favorable for the formation of hydroxyapatite. It can be seen from Figure 4d, that the carbonate-substituted apatite (HCO_3^--AP) has an irregular shape and smaller crystal grains which is consistent with the XRD results.

It should be pointed out that, under near-physiological conditions, we failed to obtain SO_4^{2-}-, HSO_4^--, or Cl^--substituted apatites by the substitution of $CaSO_4$ or $CaCl_2$ for $Ca(NO_3)_2$. In those cases, the products were always hydroxyapatite, indicating that even if SO_4^{2-}-, HSO_4^--, or Cl^--substituted apatites did exist, their solubilities in water are too high to precipitate them out from the aqueous solution. Thus, SO_4^{2-}, NO_3^-, and Cl^- have no effect on the composition of bone.

The lattice structures and parameters of the prepared substituted apatites

The substituted apatites all have orthorhombic structures with hexagonal type cells. Their unit cell dimensions and volumes are listed in Table 3.

The unit cell volumes correlate well with the ionic radii of the substituted ions. As the ionic radius of Sr^{2+} is larger

Table 5. The Removal of Low Concentrations of Heavy Metals by Substituted Apatites

Adsorbents*	Final Concentration of M ions in Solution (mg/L)†				M-Removed (%)			
	Pb^{2+}	Cd^{2+}	Hg^{2+}	Cr^{3+}	Pb^{2+}	Cd^{2+}	Hg^{2+}	Cr^{3+}
Ca-HAP	≤0.01	0.10	4.98	1.46	≥99.8	98.0	0.4	71.5
HCO_3^-–AP	≤0.01	≤0.01	1.12	≤0.01	≥99.8	≥99.8	77.6	≥99.8
$Ca_3(PO_4)_2$	≤0.01	≤0.01	1.67	≤0.01	≥99.8	≥99.8	66.7	≥99.8
$CaCO_3$	--	--	--	≤0.01	--	--	--	≥99.8

*Amount of adsorbents = 0.1 g, total volume of solution = 50 mL, exchange time = 2 h, temperature = 20°C, M = Pb, Hg, Cd, or Cr, pH 6–7.
†Initial concentration: $c\ (Pb^{2+}) = c\ (Cd^{2+}) = c\ (Hg^{2+}) = c\ (Cr^{3+}) = 5.0$ mg/L.

Table 6. The Removal of $Cr_2O_7^{2-}$ and CrO_4^{2-} by Amino-Containing Resins

Adsorbents*	Exchange Time (h)	Final Concentration of Cr in Solution (mg/L)†		Cr-Removed (%)	
		In $K_2Cr_2O_7$ Solution	In K_2CrO_4 Solution	In $K_2Cr_2O_7$ Solution	In K_2CrO_4 Solution
D380	2	2.95	5.95	84.7	66.9
	24	0.86	0.98	95.5	94.6
D382	2	4.36	6.05	77.4	66.4
	24	1.08	1.38	94.4	92.3
D301T	2	7.32	6.23	62.1	65.4
	24	1.07	2.49	94.5	86.2
Chitosan	2	10.31	15.14	46.6	15.9
	24	10.31	15.14	46.6	15.9

*Amount of adsorbents = 0.1 g, total volume of solution = 50 mL, temperature = 22°C, pH 6–7.
†Initial concentration: c(Cr, in $K_2Cr_2O_7$ solution) = 19.31 mg/L, c(Cr, in K_2CrO_4 solution) = 18.01 mg/L.

than that of Ca^{2+}, the unit cell volume of the strontium-substituted apatite is larger than that of hydroxyapatite, and similarly since the ionic radius of F^- is smaller than that of OH^-, the unit cell volume of the fluoride-substituted apatite is smaller than that of hydroxyapatite. It should be noted that although the ionic radius of HCO_3^- is larger than that of OH^-, the unit cell volume of the carbonate-substituted apatite is smaller and the c-axis lattice constant is almost the same as that for hydroxyapatite. As HCO_3^- is much larger than OH^-, it is difficult for HCO_3^- to substitute for OH^-, and so only the $-O^-$ in the structure enters into the lattice sites that were originally occupied by OH^-. The other atoms are not in the lattice and this may be why the carbonate-substituted apatite is less crystalline and has smaller crystal grains than hydroxyapatite. The $-O^-$ has a smaller radius than that of OH^- but a larger radius than that of F^-, so, the unit cell volume of the carbonate-substituted apatite is smaller than that of hydroxyapatite, but larger than that of the fluoride-substituted apatite.

Comparison of the fixation of heavy metals by the substituted apatites

To determine the sites that have the strongest ability to fix heavy metals (i.e., the key species for binding heavy-metals) in bone, a comparison of the ability of the hydroxyapatite and the substituted apatites to remove heavy metals was made. The magnesium phosphate was not studied because of its high solubility in water. The results for the hydroxyapatite, the substituted apatites, $Ca_3(PO_4)_2$ and $CaCO_3$ are shown in Table 4. In addition, another biomimetic material with a protein-resembling structure, polyaspartate hydrogel, was also studied for contrast.

The following conclusions can be drawn from Table 4:

(1) PO_4^{3-} is a very strong species for the fixation of Pb^{2+} and Cd^{2+}.

(2) Ca^{2+} and CO_3^{2-} are key species for the fixation of Cr^{3+}.

(3) With both PO_4^{3-} and CO_3^{2-} sites, the carbonate-substituted apatite exhibits a strong fixation of Pb^{2+}, Cd^{2+}, and Cr^{3+}. Compared to the polyaspartyl polymer (a protein-like structure) which has been used as a biomimetic material,[17] the carbonate-substituted apatite had lower equilibrium concentrations of Pb^{2+}, Cd^{2+}, and Cr^{3+}.

(4) The substituted apatites have some ability to fix Hg^{2+} but are better at fixing Pb^{2+}, Cd^{2+}, and Cr^{3+}.

(5) The substituted apatites have no ability to fix As^{3+}in the form of $H_3AsO_3/HAsO_2$, or Cr^{6+} in the forms of $Cr_2O_7^{2-}$ or CrO_4^{2-}.

(6) The substitution of F^- for OH^- in hydroxyapatite reduces its ability to fix Pb^{2+}, Cd^{2+}, and Cr^{3+}.

Many adsorbents exhibit excellent abilities for binding heavy-metals at high concentrations, but these same adsorbents are ineffective at removing low concentrations of heavy-metals. This is because they do not strongly bind the heavy metals, which limits the amount of heavy metal ions which can be removed. Some adsorbents from Table 4 with excellent heavy metal fixing abilities were selected and their abilities to remove heavy metals at a low concentration (5 mg/L) were investigated. The results are shown in Table 5.

It can be seen from Table 5 that calcium phosphate and the carbonate-substituted apatite still exhibit a strong fixation of Pb^{2+}, Cd^{2+}, and Cr^{3+} at low ion concentrations. These ions are almost completely removed. For Hg^{2+}, there was a smaller percentage removed at the lower concentration than at the higher concentration. This is because the formed mercury-containing phosphate compounds are slightly soluble in water which limits the amount of mercury that can be removed.

The removal of Cr (VI) in the forms of $Cr_2O_7^{2-}$ and CrO_4^{2-}

Table 4 shows that the phosphates do not fix $Cr_2O_7^{2-}$ or CrO_4^{2-} at all. In addition to phosphates, bones also contain proteins with various amino-groups.[18,19] To investigate the interaction of Cr(VI) with these functional groups, resins containing either primary-, secondary-, or tertiary-amino-groups were used to simulate similar groups in proteins and their abilities to fix Cr(VI) were examined. The results are shown in Table 6.

It can be seen from Table 6 that all the amino-containing resins remove Cr(VI) under near-neutral conditions. Chitosan is an effective agent for the removal of Cr(VI) in acidic conditions,[32] but under near-neutral condition it is not very

Table 7. Removal of Arsenic from a Solution with Other Heavy-Metal Cations*

Adsorbents*	Final Concentration of M in Solution (mg/L)†					M-Removed (%)				
	Pb^{2+}	Cd^{2+}	Hg^{2+}	Cr^{3+}	As^{3+}‡	Pb^{2+}	Cd^{2+}	Hg^{2+}	Cr^{3+}	As^{3+}
HCO_3^-AP	≤0.01	≤0.01	1.16	≤0.01	28.11	≥99.0	≥99.0	94.2	≥99.0	9.3
$Ca_3(PO_4)_2$	≤0.01	≤0.01	1.66	≤0.01	26.14	≥99.0	≥99.0	91.7	≥99.0	15.7

*Amount of adsorbents = 0.1 g, total volume of solution = 50 mL, exchange time = 2 h, temperature = 19°C, M = Pb, Hg, Cd, Cr, or As, pH 6–7.
†Initial concentration: c (Pb^{2+}) = c (Cd^{2+}) = c (Hg^{2+}) = c (Cr^{3+}) = 0.1 mmol/L, c (As^{3+}) = 30.99 mg/L.
‡As^{3+} was mainly in the form of $H_3AsO_3/HAsO_2$.

Table 8. The Removal of Arsenic by Amino-Containing Resins*

Adsorbents*	Exchange Time (h)	Final Concentration of As in Solution (mg/L)†		As-Removed (%)	
		As((III)	As (V)	As((III)	As (V)
D380	2	30.16	21.87	0.0	27.2
	24	30.16	5.17	0.0	82.8
	24	–	1.39‡	–	46.7
D301T	2	30.16	24.18	0.0	19.5
	24	30.16	5.66	0.0	81.2
	24	–	1.26‡	–	51.7
Chitosan	2	30.16	30.05	0.0	0.0
	24	30.16	28.85	0.0	4.0
HCO_3^-–AP	2	30.16	29.12	0.0	3.1
	24	30.16	28.64	0.0	4.7
$Ca_3(PO_4)_2$	2	30.16	29.32	0.0	2.4
	24	30.16	29.34	0.0	2.4

*Amount of adsorbents = 0.1 g, total volume of solution = 50 mL, temperature = 25°C, pH 6–7.
†Initial concentration: c(As(III)) = 30.16 mg/L, c (As (V)) = 30.05 mg/L.
‡Initial concentration: c (As (V)) = 2.61 mg/L.

effective. The mechanism for the removal of Cr(VI) by the amino-containing resins will be discussed in a later section.

The removal of arsenic

As shown in Table 4, the phosphates did not fix As(III). So, another test was designed to test whether arsenic could be removed from a solution containing several different heavy metal-ions. The results are shown in Table 7. The same resins used to remove Cr(VI) were also tested for their ability to fix arsenic. These results are shown in Table 8.

It can be seen from Table 7 that in the presence of Pb, Cd, Hg, and Cr, some As(III) can be removed, but the percentage is still very low. Table 8 shows that the amino-containing resins do not adsorb As(III) and have a moderate ability to remove As(V). However, at a low As(V) concentration, the percent removed is smaller than it is for a higher concentration. These results may be attributed to the different acidities of the As(III)- and As(V)-containing species. In a near-neutral aqueous solution, As(V) is mainly in the forms of $H_2AsO_4^-$ or $HAsO_4^{2-}$. The dissociation constant of $H_2AsO_4^-$ at 25°C ($K_a = 1.0 \times 10^{-7}$) is greater than that of H_3AsO_3 (or $HAsO_2$) ($K_a = 6.0 \times 10^{-10}$),[33–35] implying that $H_2AsO_4^-$ has a stronger acidity than H_3AsO_3 (or $HAsO_2$), and thus, has a stronger interaction with the alkaline amino-groups on the resins This interaction also drives the solution equilibrium between $H_2AsO_4^-$ and $HAsO_4^{2-}$ toward $H_2AsO_4^-$ which favors more As(V) being adsorbed onto the resins. However, this acid–base interaction between them is not strong enough to lead to a high removal percentage at a low concentration. A further discussion is given below.

Table 9. The Equilibrium Concentrations of Ca and P for Different Adsorbents in Water

Adsorbents	n(Ca)/n(P) in Absorbents (mol/mol)	c(Ca) in Solution (mg/L)	c(P) in Solution (mg/L)
$Ca_3(PO_4)_2$	1.51	0.86	1.96
Ca-HAP	1.68	0.84	0.94
HCO_3^--AP	1.61	3.12	4.38

Temperature = 20°C, pH ~ 7, 24 h.

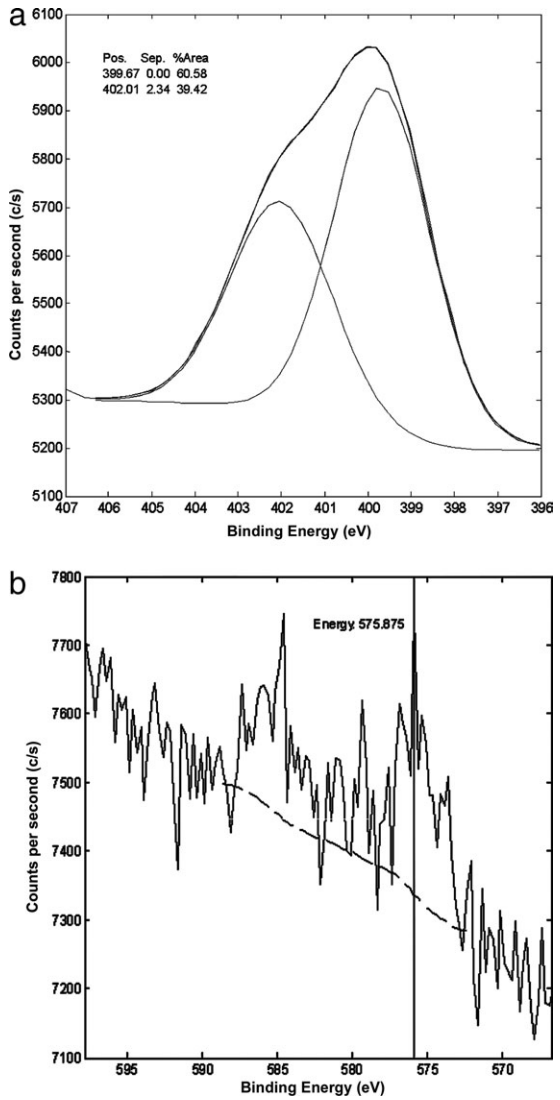

Figure 5. XPS spectra of D380 resin after adsorption of Cr(VI) (a) N1s (b) Cr $2p_{3/2}$.

The mechanism for the removal of heavy-metal ions

Mechanism for the Removal of Heavy-Metal Cations. If a water-insoluble precipitate is formed during the reaction of a heavy-metal ion and an inorganic adsorbent, the ion can be removed from aqueous solution. Ions that form precipitates with lower solubility-product constants can be removed more completely.[33] When calcium phosphate, hydroxyapatite, and carbonate-substituted apatite were used as the adsorbents for the removal of Pb^{2+}, Cd^{2+}, Hg^{2+}, and Cr^{3+}, water-insoluble compounds, such as $M_3(PO_4)_2$, $M_{10}(OH)_2(PO4)_6$, $M_{10}(HCO_3)_2(PO4)_6$, or MCO_3 (M = Pb^{2+}, Cd^{2+}, Hg^{2+}, or Cr^{3+}) were formed through an exchange with Ca^{2+} or through a reaction with PO_4^{3-} or HCO_3^-. The solubility products (Ksp) of $Ca_3(PO_4)_2$, $Pb_3(PO_4)_2$, and $Cd_3(PO_4)_2$ are 2.1×10^{-29}, 8.0×10^{-43}, and 2.5×10^{-33}, respectively,[36] implying that it is possible to substitute Pb^{2+} or Cd^{2+} for Ca^{2+}. Thus, $Ca_3(PO_4)_2$ can strongly fix Pb^{2+} and Cd^{2+}.

At a pH 7-7.2, a solution containing $Cr(OH)_3$ is turbid and a solution with a low Cr^{3+} concentration can remain suspended for 24 h. However, if Ca^{2+} and CO_3^{2-} are also both in the system, a fast precipitation will occur at the same pH and Cr^{3+} concentration. As $Cr(OH)_3$ has a low

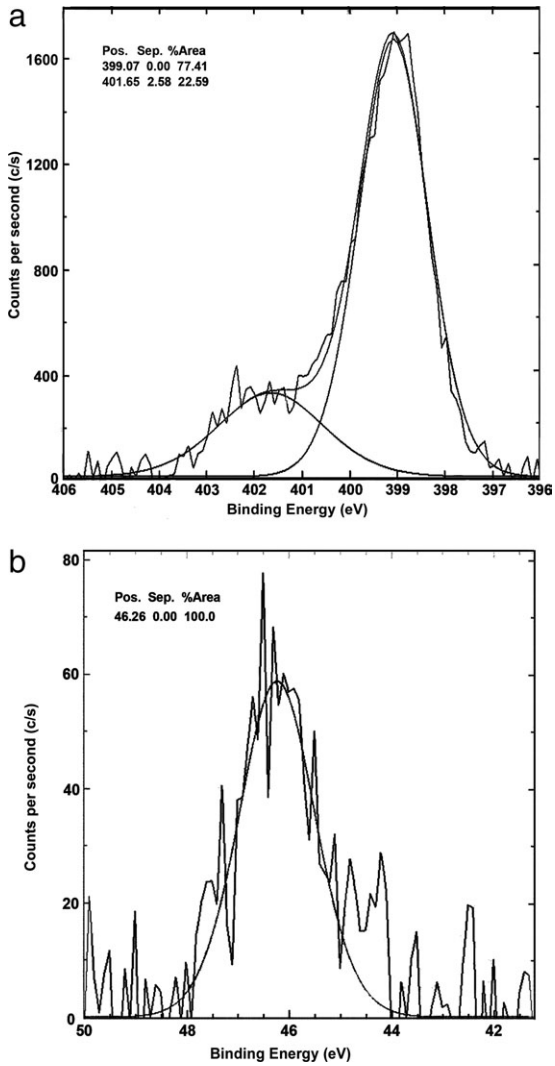

Figure 6. XPS spectra of D380 resin after adsorption of As(V) (a) N1s (b) As 3d.

solubility product (6.3×10^{-31}),[36] the strong fixation of Cr^{3+} by $CaCO_3$ can be attributed to the co-precipitation of $Cr(OH)_3$ with $CaCO_3$.

Table 9 gives the equilibrium concentration of Ca and P for different adsorbents in water. As hydroxyapatite has lower remaining concentrations of Ca and P than those for calcium phosphate or the carbonate-substituted apatite, the concentrations of Ca and P in the saturated solutions of the latter two are over-saturated compared to those in the solution of hydroxyapatite. This leads to the formation of hydroxyapatite and subsequent re-deposition on $Ca_3(PO_4)_2$ or on the carbonate-substituted apatite adsorbents.

Mechanism for the Removal of Cr(VI) and As(V). Using the D380 resin as a representative amino-containing resin, XPS was performed to investigate the removal mechanism for Cr(VI) and As(V). The results are shown in Figures 5 and 6. After adsorbing Cr(VI), the N (1s) peak of the D380 resin was separated into two Gaussian peaks centered at 399.67 and 402.01 eV (Figure 5a). A shift to higher binding energies indicates that a portion of the N atoms was oxidized. The peak at 399.67 eV is from the N atoms in $-NH_2$, and the peak at 402.01 eV can be assigned to the N atoms oxidized by Cr(VI). This suggests that the fixation of Cr(VI) on the amino-containing resin is mainly via a redox-reaction between $-NH_2$ and Cr(VI), followed by the fixation of Cr(III). The peak at 575.87 eV in the Cr ($2p_{3/2}$) spectrum (Figure 5b) may be due to Cr(III) in the form of $Cr(OH)_3$ which serves as further supporting evidence for above proposed mechanism. The precipitation of Cr(III) would cause a high formal potential (or conditional potential) for the Cr(VI)/Cr(III) couple, and thus, drive the redox-reaction nearly to completion.[33] Thus, it can be concluded that the removal of Cr(VI) is greatly improved by its reduction to Cr(III).

Figure 6 shows the XPS spectra for the D380 resin after As(V) adsorption. The N(1s) peak was separated into two Gaussian peaks centered at 399.07 and 401.65 eV (Figure 6a). The peak at 399.07 eV is from the N atoms in $-NH_2$, and the peak at 401.65 eV can be assigned to the N atoms that are interacting with the As(V) species. In the As (3d) spectrum (Figure 6b), the peak at 46.26 eV coincides with the binding energy of As(V) atoms, which serves as further evidence of the interactions between the $-NH_2$ groups in the resin and the As(V) species.

Characterization of the chitosan-polyaspartyl polymer bone–like composite and its fixation of heavy metals

As mentioned earlier, the carbonate-substituted apatite had the strongest fixation of heavy-metal cations (Pb^{2+}, Cd^{2+}, Cr^{3+}, and Hg^{2+}) and the material with primary-amino-groups has some ability to remove $Cr_2O_7^{2-}$ and CrO_4^{2-}. A large surface area is also important for the uptake of adsorbents. So, a bone-like composite was prepared, in which chitosan served as the saccharide portion, a polyaspartyl polymer as the protein portion, and the carbonate-substituted apatite as hydroxyapatite. The designed composite is expected to possess several heavy-metal-fixing groups, a large surface area, and good hydrophilicity and permeability. Thus, it should be a more effective agent than those with only one type of function group. The effects of the operating conditions and the ratios of starting materials on the composition of the composites are currently under investigation in our laboratory. The IR spectrum (Figure 1f) of the composite prepared under the conditions given in the Experimental section shows a band around 1640 cm^{-1} which can be attributed to a combination of the amide-I band (C=O stretching), the C=N stretching vibration, the amide-II band (N—H bending) and the C—N stretching vibration in the secondary

Table 10. Performance of the Composite for Removing Heavy Metal Ions*

Heavy-Metal Ions	Initial Concentration of M in Solution (mg/L)	Final Concentration of M in Solution (mg/L)	M-Removed (%)
Pb^{2+}	99.5	≤0.01	≥99.9
	5.0	≤0.01	≥99.8
Cd^{2+}	54.0	0.38	99.3
	5.0	≤0.01	≥99.8
Hg^{2+}	96.3	6.07	93.7
	5.0	0.09	98.2
	1.0	≤0.01	≥99.0
Cr^{3+}	25.0	0.33	98.7
	5.0	≤0.01	≥99.8
$Cr^{6+\dagger}$	19.2	18.1	5.7

*Amount of bone-like composite = 0.1 g, total volume of solution = 50 mL, exchange time = 2 h, temperature = 18°C, M = Pb, Hg, Cd, or Cr, pH 6–7.
†Cr^{6+} was added in the form of $Cr_2O_7^{2-}$.

amide. The band at 1400 cm^{-1} is assigned to symmetric stretching of the carboxylate anion (Vs,coo-),[16] and the strong band at 1031 cm^{-1} is due to PO_4^{3-} stretching. Additionally, the strong broad band at 3424 cm^{-1} is a combination of O—H and N—H stretching band. It can be concluded that a composite material containing chitosan and polyaspartyl polymer was formed.

The surface morphology (not shown) of the composite shows that it has nano-size particles (ca. 10–20 nm), indicating that the addition of the polyaspartyl polymer helped to disperse the inorganic phase. This is because of the interactions between $-COO^-$ and Ca^{2+}. The ability of the composite to remove heavy metal ions was examined and is shown in Table 10.

Table 10 shows that the composite exhibits excellent performance for the removal of Pb^{2+}, Cd^{2+}, and Cr^{3+}, and compared to Table 5, the removal of Hg^{2+} is improved which can be attributed to the larger surface area and the introduction of the $-COO^-$ groups in the polyaspartyl polymer structure. There are a large number of $-COO^-$ groups in the polyaspartyl polymer structure. However, the removal of $Cr_2O_7^{2-}$ is still not very effective.

Conclusions

Hydroxyapatite and some substituted-apatites, including strontium-, fluoride- and carbonate-substituted apatites, were prepared under near-physiological conditions and characterized by means of ICP, FT-IR, XRD, TG-DTA, and SEM. The experimental investigation for the removal of Pb, Cd, Hg, and Cr ions showed that the carbonate-substituted apatite exhibits a very strong ability to fix Pb^{2+}, Cd^{2+}, and Cr^{3+}.

A bone-like composite, in which chitosan served as the saccharide portion and a polyaspartyl polymer as the protein portion, was synthesized via co-precipitation. At a low heavy-metal ion concentration, under a near-neutral conditions, the biomimetic composite was excellent at removing Pb^{2+}, Cd^{2+}, Hg^{2+}, and Cr^{3+}, with removal percentages as high as 99.8% and residual concentrations as low as 0.01 mg/L. The prepared apatites had little ability to fix Cr(VI) in the form of $Cr_2O_7^{2-}$ or CrO_4^{2-}, or to fix As(III) in the form of H_3AsO_3/$HAsO_2$. However, if Cr(VI) was reduced to Cr(III), the amount removed was greatly improved. The amino-containing materials exhibited a strong ability to remove Cr(VI) and moderate adsorption of As(V) under near-neutral conditions. The mechanism of Cr(VI) removal involves a redox-reaction and then the formation of water-insoluble compounds (a precipitate).

Acknowledgments

This work was financially supported by the National Natural Science Foundation of China (20976134) and Natural Science Foundation of Tianjin (12JCYBJC13700).

Literature Cited

1. Jomova K, Valko M. Advances in metal-induced oxidative stress and human disease. *Toxicology* 2011;283:65–87.
2. Yedjou CG, Milner JN, Howard CB, Tchounwou PB. Basic apoptotic mechanisms of lead toxicity in human leukemia (Hl-60) cells. *International J Environ Res Publ Health.* 2010;7:2008–2017.
3. Messner B, Bernhard D. Cadmium and cardiovascular diseases: cell biology, pathophysiology, and epidemiological relevance. *Biometals* 2010;23:811–822.
4. Haase H, Engelhardt G, Hebel S, Rink L. Mercuric ions inhibit mitogen-activated protein kinase dephosphorylation by inducing reactive oxygen species. *Toxicol Appl Pharmacol.* 2011;250:78–86.
5. Jomova K, Jenisova Z, Feszterova M, Baros S, Liska J, Hudecova D, Rhodes CJ, Valko M. Arsenic: toxicity, oxidative stress and human disease. *J Appl Toxicol.* 2011;31:95–107.
6. Tkaczyk C, Huk OL, Mwale F, Antoniou J, Zukor DJ, Petit A, Tabrizian M. Investigation of the binding of Cr(III) complexes to bovine and human serum proteins: a proteomic approach. *J Biomed Mater Res A.* 2010;94:214–222.
7. Alp O, Merino EJ, Caruso JA. Arsenic-induced protein phosphorylation changes in HeLa cells. *Anal Bioanal Chem.* 2010;398:2099–2107.
8. Bolt AM, Douglas RM, Klimecki WT. Arsenite exposure in human lymphoblastoid cell lines induces autophagy and coordinated induction of lysosomal genes. *Toxicol Lett.* 2010;199:153–159.
9. Brzóska MM, Rogalska J, Kupraszewicz E. The involvement of oxidative stress in the mechanisms of damaging cadmium action in bone tissue: a study in a rat model of moderate and relatively high human exposure. *Toxicol Appl Pharmacol.* 2011;250:327–335.
10. Nemmiche S, Chabane-Sari D, Kadri M, Guiraud P. Cadmium chloride-induced oxidative stress and DNA damage in the human Jurkat T cell line is not linked to intracellular trace elements depletion. *Toxicology In Vitro.* 2011;25:191–198.
11. Moulis J-M. Cellular mechanisms of cadmium toxicity related to the homeostasis of essential metals. *Biometals* 2010;23:877–896
12. Lavery TJ, Kemper CM, Sanderson K, Schultz CG, Coyle P, Mitchell JG, Seuront L. Heavy metal toxicity of kidney and bone tissues in South Australian adult bottlenose dolphins (Tursiops aduncus). *Mar Environ Res.* 2009;67:1–7.
13. Yen CC, Ho TJ, Wu CC, Chang CF, Su CC, Chen YW, Jinn TR, Lu TH, Cheng PW, Su YC, Liu SH, Huang CF. Inorganic arsenic causes cell apoptosis in mouse cerebrum through an oxidative stress-regulated signaling pathway. *Arch Toxicol.* 2011;85:565–575.
14. Harrison JJ, Rabiei M, Turner RJ, Badry EA, Sproule KM, Ceri H. Metal resistance in Candida biofilms. *FEMS Microbiol Ecol.* 2006;55:479–491.
15. Sharma S, Sundaram CS, Luthra PM, Singh Y, Sirdeshmukh R, Gade WN. Role of proteins in resistance mechanism of Pseudomonas fluorescens against heavy metal induced stress with proteomics approach. *J Biotechnol.* 2006;126:374–382.
16. Sun B, Mi ZT, An G., Liu G, Zou JJ. Preparation of biomimetic materials made from polyaspartyl polymer and chitosan for heavy-metal removal. *Ind Eng Chem Res.* 2009;48:9823–9829.
17. Sun B, Mi ZT, An G., Liu G. Binding of several heavy metal ions by polyaspartyl polymers and their application to some Chinese herbal medicines. *J Appl Polym Sci.* 2007;106:2736–2745.
18. Betts F, Blumenthal NC, Posner AS. Bone mineralization. *J Cryst Growth.* 1981;53:63–73.
19. LeGeros RZ, Kijkowska R, Bautista C, Legeros JP. Synergistic effects of magnesium and carbonate on properties of biological and synthetic apatites. *Connect Tissue Res.* 1995;33:203–209.
20. Rey C, Combes C, Drouet C, Glimcher MJ. Bone mineral: update on chemical composition and structure. *Osteoporos Int.* 2009;20:1013–1021.
21. King CL, Tayles N, Gordon KC. Re-examining the chemical evaluation of diagenesis in human bone apatite. *J Archaeol Sci.* 2011;38:2222–2230.
22. Cerklewski FL. Fluoride bioavailability—nutritional and clinical aspects. *Nutrition Research.* 1997;17:907–929.
23. Boskey AL, Posner AS. Conversion of amorphous calcium phosphate to microcrystalline hydroxyapatite. A pH-dependent, solution-mediated, solid-solid conversion. *J Phys Chem.* 1973;77:2313–2317.
24. Boskey AL, Posner AS. Formation of hydroxyapatite at low supersaturation. *J Phys Chem.* 1976;80:40–45.
25. Ishikawa T, Saito H, Kandori K. Fourier-transform infrared study of CO2 Adsorption on non-stoichiometric strontium hydroxyapatites. *J Chem Soc Faraday Trans.* 1992;88:2937–2942.
26. Suchanek WL, Shuk P, Byrappa K, Riman RE, TenHuisen KS, Janas VF. Mechanochemical-hydrothermal synthesis of carbonated apatite powders at room temperature. *Biomaterials* 2002;23:699–710.
27. Jha LJ, Best SM, Knowles JC, Rehman I, Santos JD, Bonfield W. Preparation and characterization of fluoride-substituted apatites. *J Mater Sci: Mater Med.* 1997;8:185–191.
28. Fábián R, Kotsis I, Zimány P, Halmos P. Preparation and chemical characterization of high purity fluorapatite. *Talanta* 1998;46:1273–1277.
29. Joris SJ, Amberg CH. The nature of deficiency in nonstoichiometric hydroxyapatites. II: spectroscopic studies of calcium and strontium hydroxyapatites. *J Phys Chem.* 1971;75:3172–3178.
30. Rodríguez-Lorenzo LM, Hart JN, Gross KA. Influence of fluorine in the synthesis of apatites. Synthesis of solid solutions of hydroxy-fluorapatite. *Biomaterials* 2003;24:3777–3785.

31. Nikcevic I, Jokanovic V, Mitric M, Nedic Z, Makovec D, Uskokovic D. Mechanochemical synthesis of nanostructured fluorapatite/fluorhydroxyapatite and carbonated fluorapatite/fluorhydroxyapatite. *J Solid State Chem.* 2004;177:2565–2574.
32. Lasko CL, Adams KH, DeBenedet EM, West PA. A simple sulfuric acid pretreatment method to improve the adsorption of Cr(VI) by chitosan. *J Appl Polym Sci*. 2004;93:2808–2814.
33. Christian GD. *Analytical Chemistry*, 6th ed.New York: Wiley, 2004, 219–260, 326–334, 365–366, 804–805.
34. Greenwood NN, Earnshaw A. *Chemistry of the Elements*, 2nd ed. Oxford: Butterworth-Heinemann, 1997, 574–575, 577
35. Muñoz-Hernández, M.-Á. *Arsenic: Inorganic chemistry*. In: King RB, *Encyclopedia of Inorganic Chemistry*, 2nd ed., 10 Vol. Set. Chichester/New York: John Wiley & Sons, Inc., 2006, 7–9.
36. Speight JG. *Lange's Handbook of Chemistry*, 16th ed. New York: McGRAW-Hill, 2005:1333–1342.

Manuscript received May 18, 2011, revision received Dec. 12, 2011, and final revision received Mar. 15, 2012.